J Nanopart Res (2021) 23: 131
https://doi.org/10.1007/s11051-021-05258-6

RESEARCH PAPER

Cobalt nanoparticles embedded in the N-doped carbon nanospheres as efficient oxygen catalysis for rechargeable flexible Zn-air batteries

Yang Li · Ranran Tang · Jun Liu · Wenhan Zhou · Juan Gao · Hongwei Wu

Received: 25 October 2020 / Accepted: 3 June 2021 / Published online: 18 June 2021

Abstract Rechargeable Zn-air batteries are considered as a promising energy storage device due to their high energy density. Nevertheless, the sluggish kinetics of the oxygen reduction reaction/oxygen evolution reaction (ORR/OER) involved in the Zn-air batteries seriously hinders their practical application. Hence, in this work, a novel and effective method is developed to synthesize ultrafine cobalt nanoparticles (about 35 nm in diameter) embedded in nitrogen-doped carbon spheres (labeled as Co/NDC). Benefiting from the uniform distribution of the ultrafine cobalt nanoparticles, the prepared Co/NDC catalyst owns a large specific surface area and abundant active sites. As shown in the electrochemical test, the Co/NDC bifunctional electrocatalyst prepared in this article exhibits advanced electrochemical performance. The Co/NDC electrocatalyst displays superior electrochemical activities with a half-wave potential of 0.76 V (vs. RHE) for ORR and a low overpotential of 460 mV at the current density of 10 $mA{\cdot}cm^{-2}$ for OER. More significantly, the integrated rechargeable liquid-state Zn-air battery (ZAB) using Co/NDC electrocatalyst as air cathode shows a peak power density up to 149 $mA{\cdot}cm^{-2}$, an open-circuit voltage (OCV) of 1.428 V and a long-term cycle stability for more than 50 h. In addition, the self-made flexible rechargeable ZABs also display excellent performance even under different bending and twisting conditions. Therefore, Co/NDC catalyst can effectively serve as a promising candidate for bifunctional electrocatalyst.

Keywords Co · N-doped carbon · Oxygen reduction reaction · Oxygen evolution reaction · Zn-air batteries · Flexible solid-state Zn-air batteries

Introduction

With the rapid growth of population and the continuous consumption of fossil energy, it is extremely significant to seek secure, high-efficiency, environmental friendly energy conversion and storage equipments (Nl et al. 2020). In recent years, the rechargeable Zn-air battery stands out from the metal-air batteries and attracts considerable interests (Cai et al. 2018; Cao et al. 2019a). Because of its high energy density (the value is up to 1086 $Wh{\cdot}kg^{-1}$), cheapness, high-efficiency, and low environmental damage, rechargeable ZABs are considered to be one of the most promising alternative energy technologies in practical applications (Cao et al. 2019b, 2019c; Chao et al. 2018). However, low energy conversion efficiency, poor durability and electrolyte leakage in liquid-state batteries are still the main problems encountered in practical applications of rechargeable ZABs. The phenomena are mainly caused by the sluggish kinetics

Y. Li (✉) · R. Tang · J. Liu · W. Zhou · J. Gao · H. Wu
School of Mechanics and Optoelectronic Physics, Anhui University of Science and Technology, Huainan 232001, People's Republic of China
e-mail: liyang800904@163.com

of the two electrochemical reactions (OER/ORR) involved in the Zn-air batteries (Chen et al. 2015, 2020b; Fang et al. 2019). As we know, precious metal platinum-based catalysts are considered as the best ORR catalysts, and Ir/Ru-based oxides are considered as the dominant oxygen evolution catalysts (Wu and Yang 2013). However, due to the expensive, poor durability, and single catalytic performance of these noble metal catalysts, the large-scale application of rechargeable ZABs in practical applications is greatly hindered. Therefore, inexpensive, noble metal free, high-efficiency and high-stability bifunctional catalysts are in urgent demand.

Recently, heteroatom (such as N, P, B, and S) (Liang et al. 2015; Wiggins-Camacho and Stevenson 2011) doped carbon materials are identified as prominent ORR electrocatalysts, the defects caused by heteroatom doping can form plenty of active sites, therefore improving the catalytic efficiency of the catalysts (Xiang et al. 2014). In various heteroatom-doped carbon materials, nitrogen-doped carbon materials have attracted extensive attentions because of their ability in promoting electron transfer and decreasing the barriers in the diffusion process (Cheng et al. 2011; Qichen, et al. 2018). What is more, transition metal-based (e.g. Co. Ni, Mo, Fe) catalysts also have superior OER performance (Bai et al. 2018; Chen et al. 2020a; Tong et al. 2017; Yi et al. 2019). Nevertheless, the rechargeable Zn-air battery requires the catalyst to have good OER and ORR performance simultaneously, which is the vital point to obtain a steady charge and discharge process. Constructing transition metal-nitrogen-doped carbon-based catalysts is the effective way to prepare bifunctional catalysts (Chao et al. 2018; Zhang et al. 2019a). Zhang's group reported the hollow nitrogen-doped carbon $NiS_{1.03}$ nanomaterial as a superior bifunctional electrocatalyst (Zhang et al. 2020). Gao et al. prepared nitrogen-phosphorus double-doped carbon nanosheets-supported cobalt boron oxide as trifunctional electrocatalyst; they also integrated this catalyst in charging Zn-air batteries and overall water electrolysis (Gao et al. 2019). Yi and co-workers reported Co-CoO-Co_3O_4/N-doped carbon derived from metal–organic framework for Zn-Air battery (Yi et al. 2019). These results indicate that the development of transition metal-nitrogen-doped carbon compounds with nanostructures is an effective way to obtain high-efficiency bifunctional catalysts (Chen et al. 2019a; Duan et al. 2020), and the electrocatalytic activity of transition metal compounds can be further improved by controlling the morphologies of the catalysts and simplifying the experimental method (Bai et al. 2018). For example, the preparation of three-dimensional nitrogen-doped carbon spheres by electrochemical hydrothermal experimental method shows superior bifunctional electrocatalyst performance in KOH alkaline electrolyte (Zhang et al. 2020).

In this work, we reasonably designed a simple method to synthesize N-doped graphitic carbon spheres (Cao et al. 2019b). Benefiting from the unique chemical materials and characteristic nanostructures (three-dimensional transition metal-nitrogen-doped carbon spheres), the prepared transition metal catalysts exhibit excellent electrocatalytic performance (Chen et al. 2019b). As the air cathode of a rechargeable ZAB, it owns a large OCV of 1.428 V, a high-peak power density of 149 $mA{\cdot}cm^{-2}$, a large specific capacity of 725 $mA{\cdot}h{\cdot}g^{-1}$, and an outstanding long-term cycle stability (more than 50 h). The Co/NDC catalyst has superior electrochemical performance than some similar catalysts, even better than precious metal catalysts. As a result, the transition metal-nitrogen-doped carbon nanospheres in the article demonstrate an ideal OER and ORR performance, and show great potential as the cathode of liquid and flexible solid-state rechargeable ZABs.

Experimental section

Synthesis of the catalyst In the experiment, 0.12 g of cobalt nitrate hexahydrate ($Co(NO_3)_2{\bullet}6H_2O$) and 1.0 g of dopamine hydrochloride were gradually added into the 80 mL mixed solution containing ethanol and deionized water (DI water) (with a ratio of 1:1) under vigorous stirring at room temperature. Then, 4.5 mL of aqueous ammonia was added dropwise into the above mixed solution. After 8 h, the mixed solution was centrifuged, and the obtained precipitate was washed several times with ethanol and deionized water, respectively. Then, the Co-precursor was obtained after drying in a freeze drier. Finally, the CO/NDC was prepared by heating the Cobalt-precursor at 900 °C for 2 h at a ramping rate of 5 $°C{\cdot}min^{-1}$ under N_2 atmosphere. As a comparison, without adding $Co(NO_3)_2{\cdot}6H_2O$, the same method

was used to prepare graphitized carbon without adding metal materials.

Structural characterization Phase structure of the prepared catalyst powder was measured by X-ray diffraction (XRD Bruker D8-ADVANCE) with an 18-kW advanced X-ray diffractometer using Cu Kα radiation. Raman spectra were examined by Raman spectroscopy (in Via-Reflex, Renishaw, UK). The microstructure of the catalyst was characterized by scanning electron microscopy (SEM, S-4800, Hitachi, Japan) and High resolution transmission electron microscopy (HR-TEM, JEM-2100, JEOL, Japan). X-ray photoelectron spectroscopy (XPS) was irradiated by a Mg Kα achromatic X-ray source (ESCALAB 250 Xi).

Electrochemical measurements All the electrochemical performance of the electrocatalyst was tested on an electrochemical workstation instrument by the representative three-electrode test system. A glassy carbon (GC) electrode (5.0 mm in diameter) was employed as a working electrode, while platinum wire and Ag/AgCl (saturated KCl) was utilized as a counter and a reference electrode, respectively. The preparation steps of the working electrode were as follows: 5.0 mg samples was added to 500-μL mixed solution including 350-μL DI water and 150-μL isopropanol under ultrasonication for 30 min to form a homogeneous catalyst ink, then added 25-μL 5 wt.% Nafion solution. Subsequently, 8-μL catalyst ink was drop-coated onto the surface of GC electrode. For comparison, the same method was used to make the commercial Pt/C and RuO_2 catalysts.

The oxygen reduction reaction performance was measured in an O_2-saturated 0.1 M KOH alkaline solution with a scan rate of 5 $mV{\cdot}s^{-1}$ and different rotation rates (400–2025 rpm). The measurement range of the polarization curve of the oxygen reduction reaction is − 0.9 to 0.2 V (vs. Ag/AgCl). For the OER evaluation, all polarization curves were tested in the 0–1 V (vs. Ag/AgCl) at 5 mV s^{-1} under the speed rate of 1600 rpm. For ORR at RDE, the following Koutecky-Levich (K-L) equation can be used to obtain the electron transfer number (n):

$$\frac{1}{j} = \frac{1}{j_k} + \frac{1}{B\times\omega^{\frac{1}{2}}} \quad (1)$$

$$B = 0.2 \times n \times F \times C_{O_2} \times D_{O_2}^{\frac{2}{3}} \times v^{-\frac{1}{6}} \quad (2)$$

where j is the tested current density, j_k is the dynamic current density, ω is the electrode rotating speed in $rad{\cdot}s^{-1}$, F is the Faradic constant (96,485 $C{\cdot}mol^{-1}$), C_{O2} is the saturation concentration of O_2 in 0.1 M KOH alkaline electrolyte (1.2×10^{-6} $mol{\cdot}cm^{-3}$), D_{O2} is the diffusion coefficient of O_2 in 0.1 M KOH alkaline solution (1.9×10^{-5} $cm^2{\cdot}s^{-1}$), v is the kinematic viscosity of the electrolyte (0.01 $cm^2{\cdot}s^{-1}$) and n is the electrode-transfer number in ORR.

Zn-air batteries assembly and measurements The self-regulated electrochemical rechargeable Zn-air cells were assembled in the current work. The black catalyst ink was dip-located on the hydrophobic carbon cloth (1 $mg{\cdot}cm^{-2}$) as the air electrode. A polished zinc sheet with a thickness of 0.5 mm as an anode, and a 6 M potassium hydroxide, and 0.2 M zinc acetate (Zn $(Ac)_2$) alkaline aqueous liquid were used as the electrolyte. All the measurements of the rechargeable Zn-air battery were tested at room temperature using LAND cell testing system. In the cycle performance test, the galvanostatic discharge/charge curves were composed of one discharge step and one charge step for a cycle of alternate discharge and charge. In each cycle, the parameters (current density and time of duration) of the charge must be consistent with the parameters of the discharge.

Results and discussion

As displayed in Fig. 1a, $Co(NO_3)_2{\bullet}6H_2O$, dopamine hydrochloride, and aqueous ammonia were successively added into the mixed solution, and the Co-precursor was synthesized via a simple method, then the Co/NDC composites were obtained through high-temperature pyrolysis under flowing N_2 atmosphere. Use the same preparation method to prepare the corresponding metal-free catalyst (The specific experimental details refer to the Experimental Section). The morphology and nanostructure of the prepared Co/NDC powder catalyst were measured by the scanning electron microscope (SEM) and transmission electron microscope (TEM) techniques. It can be clearly seen from the SEM image that the prepared Co/NDC catalyst powder is formed by agglomeration

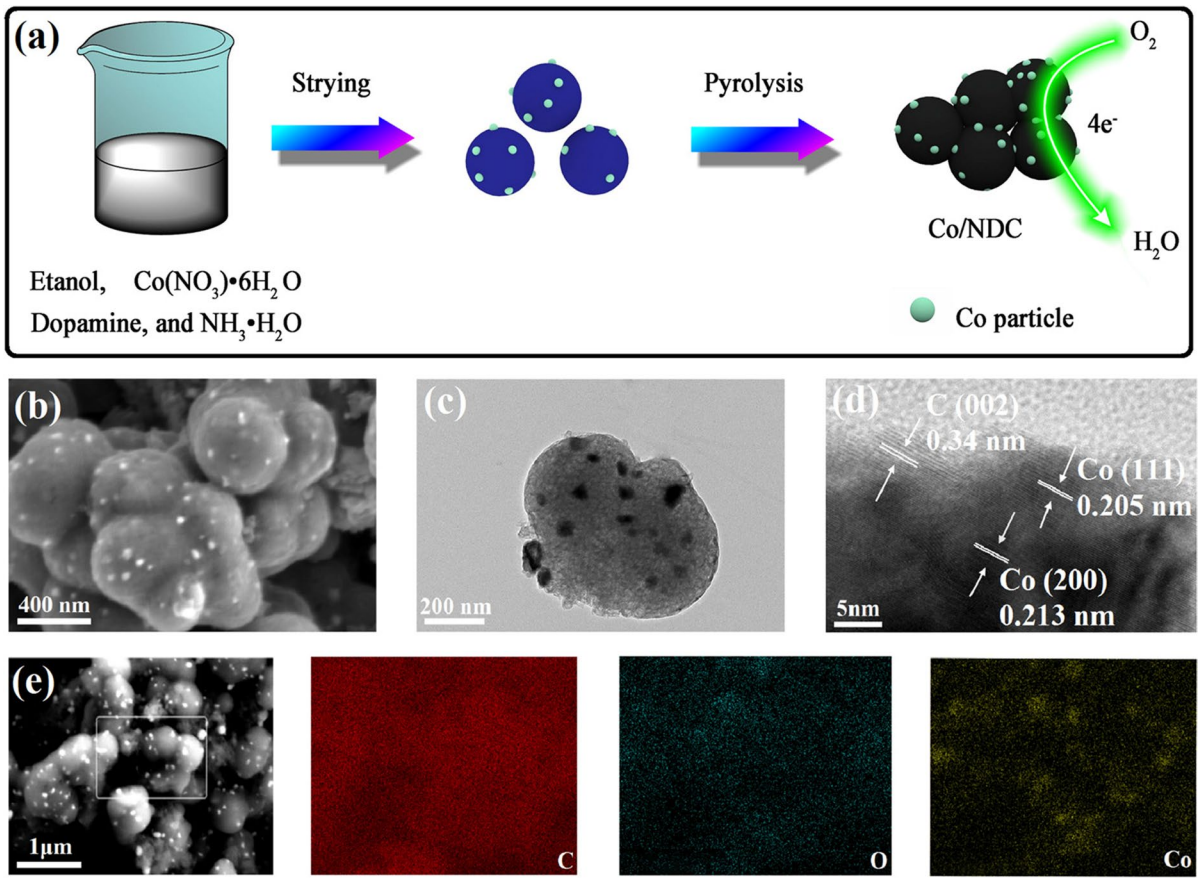

Fig. 1 **a** Schematic diagram of the synthesis process of Co/NDC catalyst. The SEM image of the microscopic morphology **b** and TEM image **c** of Co/NDC catalyst. **d** HRTEM image. **e** The corresponding EDS elemental mapping image of C, O, Co, respectively

of uniformly-sized nanospheres, and there are some uniformly distributed nanoparticles on the surface (Fig. 1b) (Huang et al. 2014; Yang et al. 2018). The nanostructure of the prepared Co/NDC powder catalyst was further investigated via TEM. We can see from Fig. 1c that the metallic cobalt (Co) nanoparticles of similar size are evenly distributed on the nanospheres, which demonstrates that the metallic Co nanoparticles are uniformly fixed on the carbon framework. The corresponding high-resolution transmission electron microscope (HRTEM) image of Co/NDC exhibited in Fig. 1d shows that the lattice distances of 0.213 nm and 0.205 nm are corresponding to the (200) and (111) crystal planes of metallic cobalt (Zhou et al. 2019), respectively, which confirmed the successful introduction of cobalt. In addition, the other visible lattice distance of 0.34 nm belonged to the (002) crystal plane of graphite carbon (Pei et al. 2019). What is more, the energy dispersive X-ray spectroscopy (EDS) mapping technology was also used to research the chemical component of the Co/NDC catalyst. It can also be seen from Fig. 1e that the carbon, oxygen, and cobalt elements are uniformly dispersed throughout the selected area, further demonstrating the successful introduction of Co species in the Co/NDC catalyst.

The crystalline structure of the as-prepared Co/NDC and NDC electrocatalysts were further analyzed by using the X-ray diffraction (XRD) pattern. As presented in Fig. 2a, these two samples also have a wide frequency band at around 26.4°, belonging to the (002) crystal planes of the graphite carbon. The other strong diffraction peaks of the Co/NDC catalyst at around 44.2°, 51.5°, and 75.8° corresponded to the (111), (200), and (220) faces of metallic Co (PDF # 15–0806), respectively. All of the above indicated the

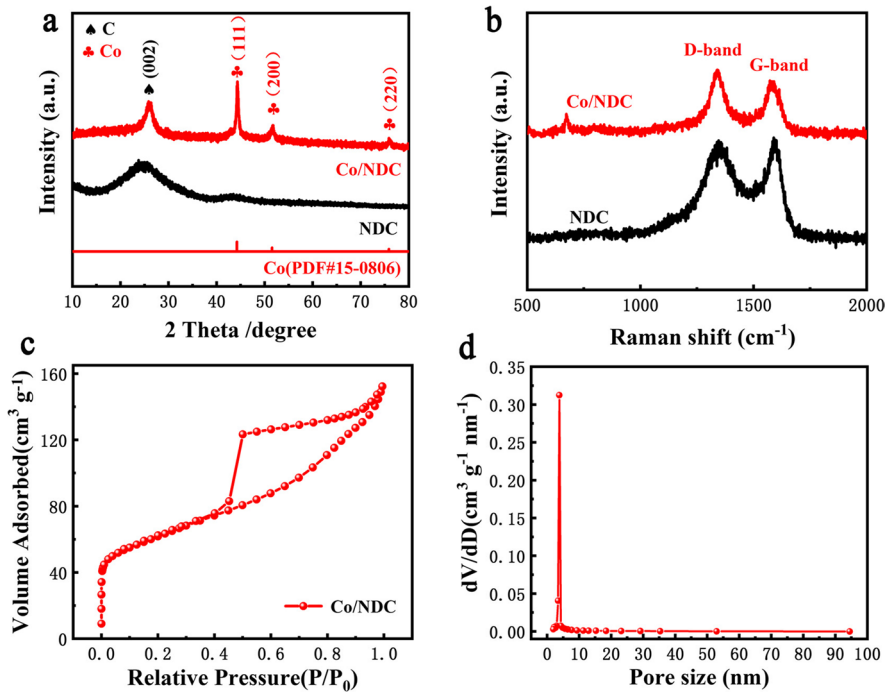

Fig. 2 **a** XRD patterns of these two samples. **b** Raman spectra of the Co/NDC and NDC catalysts. **c** N_2 adsorption–desorption isotherms. **d** Pore size distributions of Co/NDC catalyst

successful synthesis of nanocomposites (Tang et al. 2020; Wang et al. 2020; Zhou et al. 2019). What is more, the Raman spectra of the two samples further demonstrate the presence of graphite carbon in the NDC and Co/NDC electrocatalysts. As shown in Fig. 2b, in the Raman spectra of these two samples, there are two typical strong carbon peaks at approximately 1340 cm^{-1} (D band) and 1579 cm^{-1} (G band) (Goncharov et al. 2010). Besides, in the Raman spectrum of the Co/NDC catalyst, another extra peak can be obviously observed near 673 cm^{-1}, which is due to the existence of metallic Co species. These consequences further confirm the makeup of metallic Co phase in Co/NDC catalyst. In addition, with the introduction of cobalt materials, the D band value gradually increased, indicating that the active sites increased.

The Brunauer–Emmett–Teller (BET) surface area and porosity of the Co/NDC were further analyzed using N_2 adsorption–desorption isotherms. Figure 2c displays a type-IV isotherm with a distinct hysteresis loop, revealing the presence of a large number of micro/mesopores that existed in Co/NDC composites. Such hierarchically micro/mesoporous structure is also reflected by the pore size distributions (Fig. 2d). The calculated specific surface area of Co/NDC is 220 m^2 g^{-1}, as an electrocatalyst, high surface area and rich pore structure are crucial for maximizing the exposure of abundant catalytic active sites and improving the reaction kinetics, thus enhancing electrocatalytic properties.

X-ray photoelectron spectra (XPS) was used to measure the Co/NDC and NDC samples to explore the internal element composition and the chemical state of each element. Figure 3a reveals that all peaks of C, N, and O appear in the measurement spectra of the Co/NDC and NDC samples. In contrast, compared with NDC sample, there is one more Co diffraction peak in the measurement spectrum of Co/NDC sample, which supports the existence of Co particles. After measurement, the atomic weight of C, N, O and Co were 91.09%, 1.85%, 5.94%, and 1.12%, respectively (Fig. 3b). The thermal behavior of the prepared Co/NDC and NDC samples was investigated through thermal gravimetric analyzer (TGA), when the temperature increased from 30 to 800 ℃ in air (Fig. 3c). It can be seen that the Co/NDC sample underwent a drastic weight loss between 400 ℃ and 700 ℃, the mass of the remaining product was 24.4% of the original weight. As the temperature continued to rise, no weight loss was observed, indicating the complete decomposition of the organic materials in Co/NDC

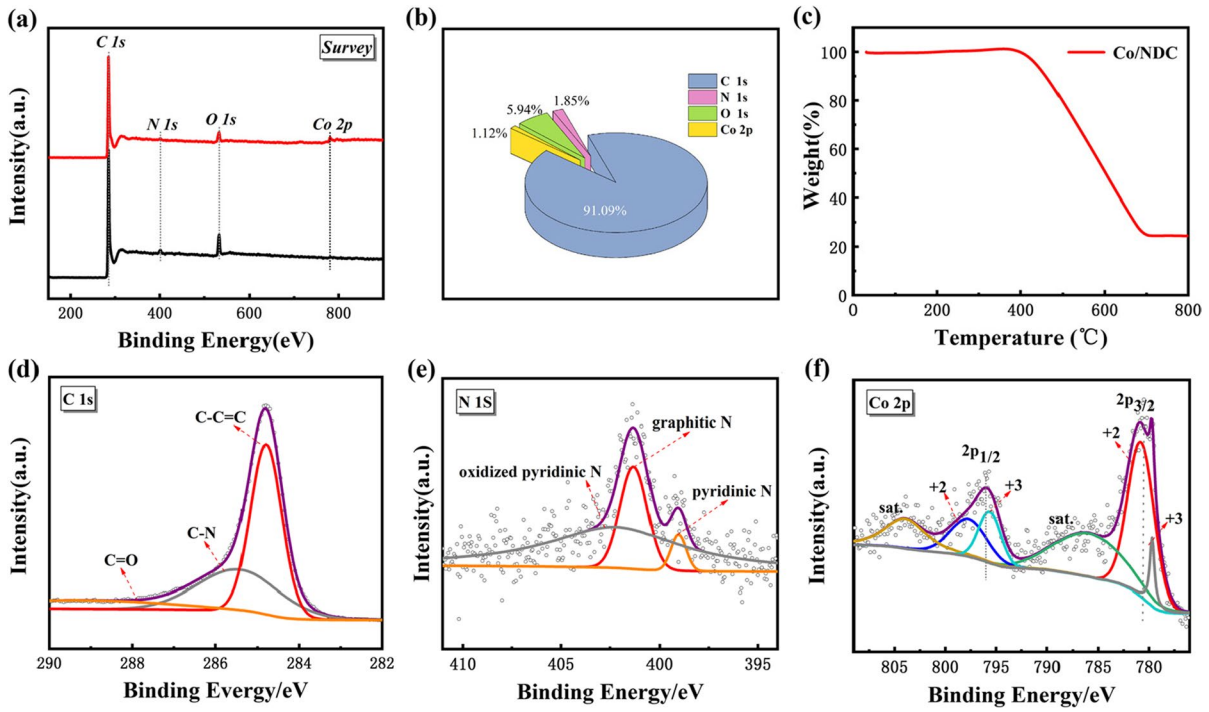

Fig. 3 The XPS spectra of the Co/NDC catalyst: **a** survey spectrum; **b** percentage of each atomic of carbon, nitrogen, oxygen and cobalt; **c** the XPS spectra of the Co/NDC catalyst: **d** C 1 s, **e** N 1 s, **f** Co 2p

and the simultaneous formation of CoO at temperatures above 700 ℃. Thus, according to the law of conservation of elements (the content of cobalt in CoO is equal to that in metallic Co), the percentage of Co and C content in the Co/NDC composite was calculated to be 19.2 wt.% and 80.8 wt.%, respectively.

The high-resolution C 1 s spectrum (Fig. 3d) can be decomposed into three peaks situated at 291.01 eV (C = O), 298.74 eV (C-N), and 284.80 eV (C–C = O) (Zhang et al. 2019a), respectively. The presence of C-N bond indicated the existence of N-doped in the graphitic carbon network. Besides, the N 1 s spectrum (Fig. 3e) of Co/NDC was decomposed into three peaks located at 402.18 eV ± 0.2 eV, 401.31 eV ± 0.2 eV, and 399.04 eV ± 0.2 eV, respectively, which can be corresponded to oxidized pyridinic N, graphitic N and pyridinic N (Liu et al. 2020; Wang et al. 2020; Zhu et al. 2019). Besides, as shown in Fig. 3f, the two pairs of characteristic peaks situated at 799.69/797.70 eV and 785.88/780.79 eV marked as Co $2p_{1/2}$ and Co $2p_{3/2}$ of the Co^{2+}/Co^{3+} species (Zhang et al. 2019c), respectively. In addition, the other two peaks at 803.95 eV and 795.62 eV correspond to satellite (Sat.) peaks (Bai et al. 2018; Chen et al. 2019a; Liu et al. 2019).

The catalysts Co/NDC and NDC were tested in 0.1 M potassium hydroxide electrolyte by using three-electrode system method to evaluate their ORR performance. The cyclic voltammetry curve of the Co/NDC catalyst was measured in 0.1 M potassium hydroxide alkaline electrolyte (0.03 V ~ − 0.77 V vs. RHE) at first. As shown in Fig. 4a, the CV curves of Co/NDC and NDC catalysts in O_2-saturated alkaline solution (solid line) exhibit obvious oxygen reduction peak, while in N_2-saturated alkaline solution (dashed line), the reduction peak disappears in the corresponding CV curves. Especially for the oxygen reduction peak potential, Co/NDC has a stronger oxygen reduction peak than NDC, indicating its outstanding ORR performance. The ORR activities of the prepared catalysts were further evaluated by using the linear scanning voltammeter (LSV) curves at 1600 rpm in 0.1 M KOH alkaline solution. As shown in Fig. 4b, the result of the Co/NDC catalyst and 20% Pt/C indicates that the onset potential of Co/NDC catalyst is 0.9 V, the value is relatively close to the commercial

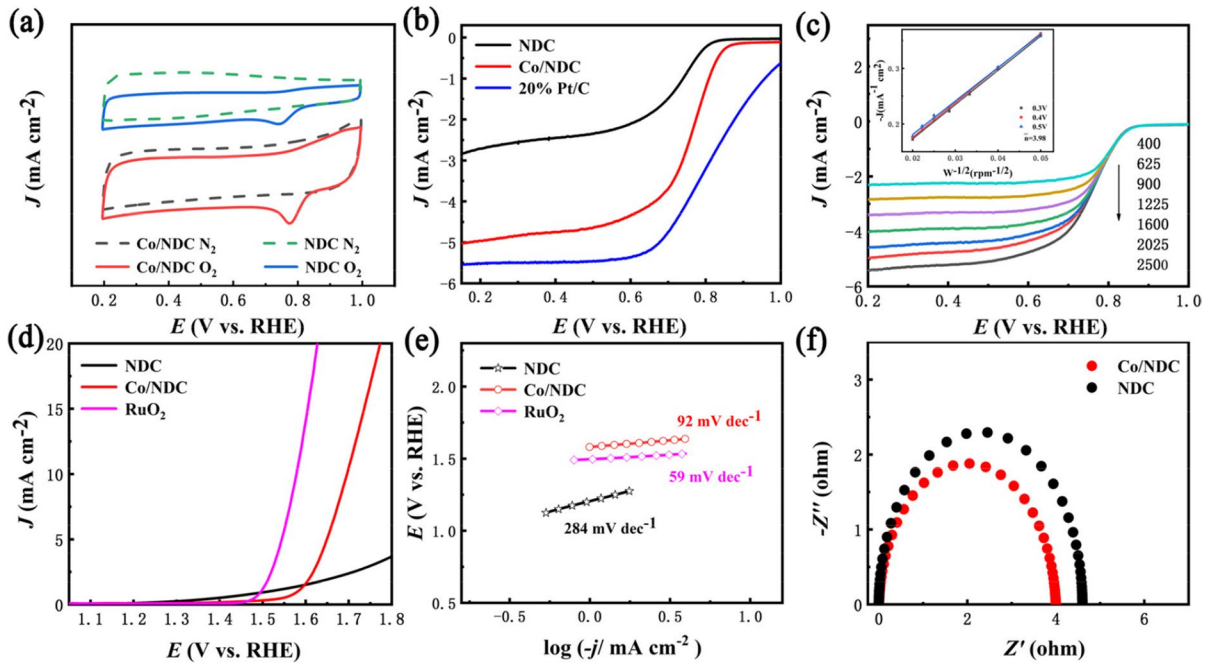

Fig. 4 Electrochemical performance of Co/NDC and NDC electrocatalysts in alkaline electrolyte: **a** CV curves in O_2 and N_2-saturated alkaline solution at a scan rate of 200 mV s^{-1}. **b** ORR LSV curves of the commercial Pt/C, Co/NDC, and NDC electrocatalysts. **c** K-L plots of Co/NDC electrocatalyst for different potentials, and the ORR polarization curves (insert image) of Co/NDC catalyst at a scan rate of 5 mV s^{-1} and at different rates (range from 400 to 2500 rpm). **d** OER LSV curves of the commercial RuO_2, Co/NDC, and NDC catalysts. **e** The corresponding Tafel plots. **f** EIS plots of Co/NDC and NDC catalysts at the open-circuit potential

20% Pt/C (0.99 V), but higher than the value of NDC catalyst. In addition, the half-wave potential of Co/NDC catalyst is 0.76 V, which is 60 mV lower than that of 20% Pt/C, but higher than that of NDC catalyst (0.7 V). What is more, the Co/NDC catalyst exhibits the large diffusion limited current density of 5 mA cm^{-2}, which is merely 0.5 mV lower than the commercial Pt/C catalyst, but much higher than the NDC catalyst (2.8 mA cm^{-2}). The outstanding catalytic activity of the Co/NDC catalyst implies that it has a high electron transfer efficiency in the ORR reaction. The LSV curves of the Co/NDC catalyst at different rotation speeds (400–2500 rpm) were tested in Fig. 4c to investigate the electron transfer number of ORR. It can be clearly seen that as the speed increases, the corresponding limiting current density is also enhanced. What is more, the Koutecky–Levich (K–L) plots based on LSVs (inset in Fig. 4c) at different rotation speeds show a good linear relationship (Wang et al. 2019). After calculation, the number of electrons transfer is about 3.98, which is close to 4 (Fig. 4c), indicating a direct 4-electron transfer pathway of Co/NDC catalyst toward the ORR. For bifunctional electrocatalysts used in charge/discharge ZABs, in addition to the electrochemical performance of ORR, the electrochemical performance of OER is also very significant. Thus, we also used the three-electrode test system method to evaluate their oxygen evolution reaction performance in 1 M KOH alkaline electrolyte. As shown in Fig. 4d, the LSV curve of the Co/NDC catalyst in alkaline electrolyte has a smaller overpotential of 0.46 V at the current density of 10 mA cm^{-2}, which is less than that of NDC catalyst, but it is very close to the commercial RuO_2 catalyst, demonstrating that the Co/NDC catalyst has higher OER activity. In addition, the high OER activity of the Co/NDC catalyst can also be seen from its low Tafel slope of 92 mV dec^{-1}, which is much approaching to the commercial RuO_2 (59 mV dec^{-1}) (Fig. 4e). Simultaneously, the electrochemical impedance spectroscopy (EIS) method further proved that the prepared Co/NDC catalyst has excellent kinetic activity

in alkaline electrolyte. It can be seen from Fig. 4f that the Co/NDC catalyst has a small charge transfer resistance (The diameter of the semicircle in the high frequency zone corresponds to the overall resistance between the electrode and the electrolyte interface). A table was made to compare the bifunction electrocatalytic performance of the OER and ORR in this study with catalysts reported in recent years showed in Table 1.

Considering the superior bifunctional OER/ORR electrocatalytic performance, we used the Co/NDC bifunctional catalyst coated on carbon cloth (1 mg/cm^2) as the air cathode to fabricate a rechargeable liquid-state Zn-air battery (Zhang et al. 2019a). Besides, the Zinc flakes and the alkaline solution (mixture aqueous solution of 6 M KOH and 0.2 M $Zn(Ac)_2$) were used as the anode and electrolyte of the liquid-state rechargeable ZABs, respectively. For comparison, we also self-assembled liquid ZAB using a commercial mixed Pt/C + RuO_2 catalyst as the air cathode. The OCV of the battery based on Co/NDC catalyst is stable at 1.428 V, which is close to 1.479 V corresponding to Pt/C + RuO_2 (Fig. 5a). As illustrated in Fig. 5b, the discharge power density curves of the Zn-air batteries with the Co/NDC electrocatalyst and Pt/C + RuO_2 hybrid catalyst and the corresponding discharge power density at different current densities. The peak power density of the Co/NDC-based Zn-air battery is 149 mW/cm^2 (at a current density of 196.4 mA/cm^2), which is higher than the commercial mixed Pt/C + RuO_2 catalyst (114.5 mW/cm^2 at about 187.4 mA/cm^2). This is because the active Co nanoparticles are completely exposed, thereby generating higher power. Moreover, according to Fig. 5c, the related voltage values of charging and discharging at the current density of 50 mA/cm^2 for the ZABs made with Co/NDC catalyst as the air cathode are 2.204 V and 1.096 V, corresponding to the mixed Pt/C + RuO_2 catalyst (2.269 V and 1.096 V). The Co/NDC-based ZABs show a smaller voltage gap, indicating that Co/NDC-based batteries have better reversibility. In order to prove that the Zn-air battery has superior electrochemical cycle stability, we did a charge–discharge cycle test (one cycle of 20 min). Figure 5d shows that the voltage gap of the Co/NDC-based battery has no significant change after running for more than 50 h (150 cycles). However, after about 30 h of Pt/C + RuO_2-based battery cycle, the voltage gap has changed greatly. Figure 5e shows that the Co/NDC based battery under different current densities, after 5 h of galvanostatic discharge test, the voltage gap did not change obviously, indicating the superior stability of Co/NDC catalyst as an air cathode. Furthermore, the specific capacity can reach up to 795 mAh/g of the Co/NDC-based battery at a current density of 10 mA/cm^2 (Fig. 5f). In addition, an electro luminescence panel can be lighted by three serious-connected Co/NDC-based liquid-state Zn-air batteries (Fig. 5g). All the above electrochemical tests strongly elucidate that Co/NDC catalyst has superior ORR/OER bifunction electrochemical performance. In order to explore the application of flexible devices of Zn-air batteries in actual production activities, we made up solid-state flexible ZABs by using the Co/NDC catalyst as the air cathode (Fig. 5h) (Zhang et al. 2018), a red LED bulb was powered by two series-connected flexible solid-state batteries. Figure 5i shows that the OCV of the Co/NDC-based solid-state ZAB is 1.401 V. Compared with liquid batteries, the solid-state ZAB also has better cycle stability. Bending at different angles

Table 1 Comparison of the bifunction electrocatalytic performance of the OER and ORR in this study with catalysts reported in recent years

Catalyst	$E_{1/2}$/V	J_L ($mA\ cm^{-2}$)	$E_{(j=10)}$/V	Ref
Co/NDC	0.76	5.0	1.69	This work
20% Pt/C	0.82	5.5	N.A	This work
RuO_2	N.A	N.A	1.6	This work
Fe-NDC	0.84	5.5	> 1.9	Zhang et al. 2019b)
O-Co_3O_4@MCN	0.76	3.5	1.66	Nl et al. 2020)
1 nm CoO_x	0.89	6.0	1.6	Wang et al. 2019)
Co/Co_xM_y	N.A	N.A	1.57	Chen et al. 2019a)
Co/N–C-800	0.74	N.A	1.6	Y., Zhu, Jiang,, et al. 2014)
Co-CoO-Co_3O_4/N-doped carbon	0.80	5.12	1.63	Yi et al. 2019)

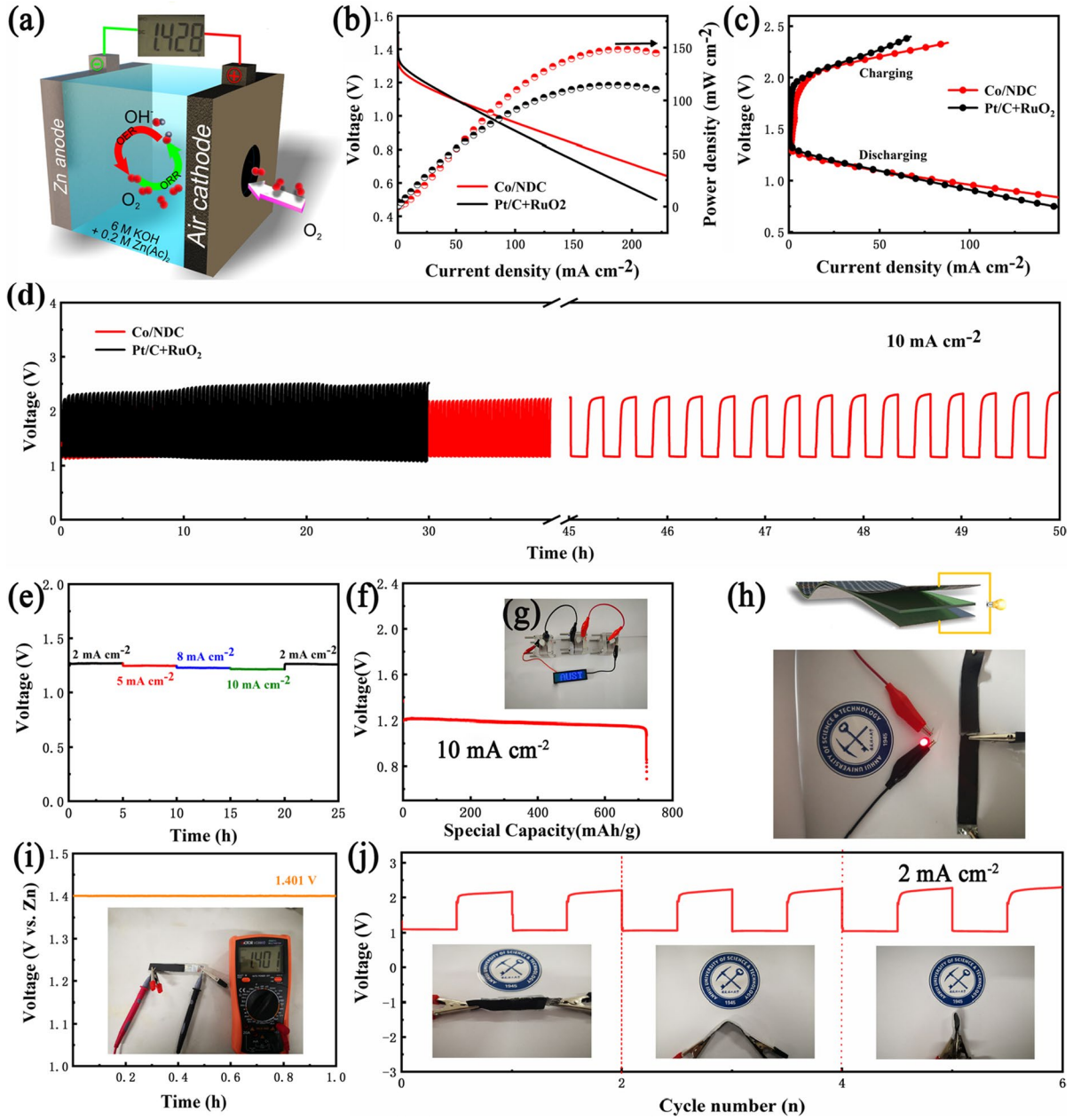

Fig. 5 **a** Schematic diagram of the self-assembled liquid-state Zn-air battery and the image of its open-circuit potential. **b** Polarization and the special power density curves of the ZAB with Co/NDC catalyst and the commercial mixed Pt/C + RuO_2 as air cathode. **c** and the corresponding charge and discharge curves. **d** Galvanostatic charge and discharge cycling performance of rechargeable liquid state ZAB based on Co/NDC (red line) and the commercial mixed Pt/C + RuO_2 (black line) electrodes at 10 mA cm^{-2}. **e** Discharge curves of ZAB with Co/NDC as the air cathode under multi-current density. **f** Special capacity of Co/NDC as cathode at 10 mA cm^{-2}. **g** Photo of an electroluminescent panel powered by three liquid-state Co/NDC-based ZABs in series. **h** A photo of a red LED bulb powered by two flexible Co/NDC-based Zn-air batteries in series. **i** The OCV of a flexible Zn-air battery. **j** Cycling activity of the flexible and rechargeable ZAB with Co/NDC as the air cathode at 2 mA cm^{-2}

(current density at 2 mA/cm^2), there is no obvious change in the voltage of the solid-state battery, which proves that the solid-state battery has good flexibility (Fig. 5j).

Conclusions

In summary, we prepared transition metal Co nanoparticles uniformly embedded in nitrogen-doped graphite carbon nanospheres through a reasonable structure design plan. The superior electrochemical activity of transition metal catalyst is attributed to its unique nanostructure and electron state. The prepared Co/NDC catalyst has a large active surface area, thereby improving the conductivity of the catalyst, as a result the Co/NDC catalyst shows outstanding electrochemical activity. The prepared Co/NDC catalyst exhibits superior ORR activity in 0.1 M KOH alkaline aqueous solution with a positive half-wave potential of 0.76 V, and a small overpotential of 0.46 mV at 10 mA·cm^{-2} in 1 M KOH alkaline aqueous solution, which exceeds NDC catalyst and close to commercial platinum carbon catalyst. In addition, the rechargeable liquid-state Zn-air battery based on the Co/NDC catalyst acquires a high-peak power density value of 149 mA·cm^{-2}, a large open-circuit voltage of 1.428 V, and a long lifetime of more than 50 h, which outperforms the commercial mixed Pt/C + RuO_2 catalyst. Besides, the self-made flexible solid-state rechargeable ZAB exhibits excellent flexibility and durability under different bending and twisting conditions. This work not only provides a reasonable structural design scheme for the preparation of high-activity ZABs and non-noble metal-based bifunctional electrocatalysts, but also enables us to have a deeper researching and understanding of the source of its intrinsic activity.

Funding This work was financed by the National Natural Science Foundation of China (Grant Nos. 51502005, 51702003, and 11904008); Anhui Provincial Quality Engineering Project (Grant Nos. 2017sxzx15, 2018zygc012); the Natural Science Foundation of Anhui Province (Grant No. 1908085QA21), and the University Natural Science Research Project of Anhui Province (Grant No. KJ2020A0328).

Declarations

Conflict of interest The authors declare that they have no conflict of interest.

References

Bai J, Meng T, Guo D et al (2018) Co9S8@MoS2 core-shell heterostructures as trifunctional electrocatalysts for overall water splitting and Zn-Air batteries. ACS Appl Mater Interfaces 10:1678–1689

Cai P, Li Y, Chen J et al (2018) An asymmetric-electrolyte Zn–Air battery with ultrahigh power density and energy density. ChemElectroChem 5:589–592

Cao Y, Zheng X, Zhang H et al (2019a) Interface engineering of NiS2/CoS2 nanohybrids as bifunctional electrocatalysts for rechargeable solid state Zn-air battery. J Power Sources 437

Cao Z, Hu H, Wu M et al (2019b) Planar all-solid-state rechargeable Zn–air batteries for compact wearable energy storage. J Mater Chem A 7:17581–17593

Cao Z, Hu H, Wu M et al (2019c) Confined growth of MoSe2 nanosheets in N-doped carbon shell with hierarchical porous structure for efficient hydrogen evolution. Sustain Energ Fuels 3:2409–2416

Chao S, Wang G, Xu D et al (2018) M (Co, Ni), N and S tridoped carbon nanoplates as multifunctional catalysts for rechargeable Zn-air batteries and water electrolyzers. Int J Hydrogen Energ 43:11012–11021

Chen P, Xu K, Fang Z et al (2015) Metallic Co4N porous nanowire arrays activated by surface oxidation as electrocatalysts for the oxygen evolution reaction. Angew Chem Int Ed Engl 54:14710–14714

Chen J, Fan C, Hu X et al (2019a) Hierarchically porous Co/Cox My (M = P, N) as an efficient Mott-Schottky electrocatalyst for oxygen evolution in rechargeable Zn-Air batteries. Small 15:e1901518

Chen M, He Y, Spendelow JS et al (2019b) Atomically dispersed metal catalysts for oxygen reduction. Acs Energy Lett 4:1619–1633

Chen K, Kim S, Rajendiran Writing Editing R et al (2020a) Enhancing ORR/OER Active sites through lattice distortion of Fe-enriched FeNi3 intermetallic nanoparticles doped N-doped carbon for high-performance rechargeable Zn-air battery. J Colloid Interf Sci

Chen Z, Zhao D, Chen C et al (2020b) Reconstruction of pH-universal atomic Fe-N-C catalysts towards oxygen reduction reaction. J Colloid Interf Sci

Cheng F, Shen J, Peng B et al (2011) Rapid room-temperature synthesis of nanocrystalline spinels as oxygen reduction and evolution electrocatalysts. Nat Chem 3:79

Duan X, Ren S, Pan N et al (2020) MOF-derived Fe, Co@N–C bifunctional oxygen electrocatalysts for Zn–air batteries. J Mater Chem A 8:9355–9363

Fang W, Hu H, Jiang T et al (2019) N- and S-doped porous carbon decorated with in-situ synthesized Co–Ni bimetallic sulfides particles: a cathode catalyst of rechargeable Zn-air batteries. Carbon 146:476–485

Goncharov VN, Sangster TC, Boehly TR et al (2010) Demonstration of the highest deuterium-tritium areal density using multiple-picket cryogenic designs on OMEGA. Phys Rev Lett 104:165001

Gao L, Zhu M, Zhang Z et al (2019) Cobalt-boron-oxide supported on N, P dual-doped carbon nanosheets as the trifunctional electrocatalyst and its application in

rechargeable Zn-air battery and overall water-electrolysis. Electrochim Acta 327

Huang S, Wu H, Zhou M et al (2014) A flexible and transparent ceramic nanobelt network for soft electronics. NPG Asia Materials 6:e86–e86

Liang JL, Qu YP, Yang CG et al (2015) Identification of QTLs associated with salt or alkaline tolerance at the seedling stage in rice under salt or alkaline stress. Euphytica 201:441–452

Liu L, Wang Y, Yan F et al (2019) Cobalt-encapsulated nitrogen-doped carbon nanotube arrays for flexible zinc–air batteries. Small Methods 4

Liu N, Hu H, Xu X et al (2020) Hybrid battery integrated by Zn-air and Zn-Co3O4 batteries at cell level. J Energy Chem 49:375–383

Nl A, Hh A, Xx A et al (2020) Hybrid battery integrated by Zn-air and Zn-Co 3 O 4 batteries at cell level. J Energy Chem 49:375–383

Pei Z, Huang Y, Tang Z et al (2019) Enabling highly efficient, flexible and rechargeable quasi-solid-state zn-air batteries via catalyst engineering and electrolyte functionalization. Energy Storage Materials 20:234–242

Qichen, Wang, Yongpeng et al (2018) Edge defects engineering of nitrogen-doped carbon for oxygen electrocatalysts in Zn-air batteries. Acs Appl Mater Inter

Tang R, Li Y, Liu J et al (2020) Cobalt nanoparticles embedded nitrogen-doped carbon nanotubes as bifunctional catalysts for flexible solid-state Zn-Air battery. J Electrochem Soc 167

Tong M, Wang L, Yu P et al (2017) Ni3S2 nanosheets in-situ epitaxially grown on nanorods as high active and stable homojunction electrocatalyst for hydrogen evolution reaction. Acs Sustain Chem Eng:acssuschemeng.7b03915

Wang X, Sunarso J, Lu Q et al (2019) High-performance platinum-perovskite composite bifunctional oxygen electrocatalyst for rechargeable zn–air battery. Adv Energy Mater 10

Wang F, Zhao H, Ma Y et al (2020) Core-shell-structured Co@Co4N nanoparticles encapsulated into MnO-modified porous N-doping carbon nanocubes as bifunctional catalysts for rechargeable Zn–air batteries. J Energy Chem 50:52–62

Wiggins-Camacho JD, Stevenson KJ (2011) Mechanistic discussion of the oxygen reduction reaction at nitrogen-doped carbon nanotubes. J Phys Chem C 115:20002–20010

Wu JB, Yang H (2013) Platinum-based oxygen reduction electrocatalysts. Acc Chem Res 46:1848–1857

Xiang Z, Cao D, Huang L et al (2014) Nitrogen-doped holey graphitic carbon from 2D covalent organic polymers for oxygen reduction. Adv Mater 26:3315–3320

Y., Zhu, Jiang et al (2014) Cobalt nanoparticles embedded in N-doped carbon as an efficient bifunctional electrocatalyst for oxygen reduction and evolution reactions. NANOSCALE -CAMBRIDGE-

Yang L, Zeng X, Wang D et al (2018) Biomass-derived FeNi alloy and nitrogen-codoped porous carbons as highly efficient oxygen reduction and evolution bifunctional electrocatalysts for rechargeable Zn-air battery. Energy Storage Materials 12:277–283

Yi X, He X, Yin F et al (2019) Co-CoO-Co3O4/N-doped carbon derived from metal-organic framework: the addition of carbon black for boosting oxygen electrocatalysis and Zn-Air battery. Electrochim Acta 295:966–977

Zhang Z, Zhou D, Bao X et al (2018) Further studies of a zinc-air cell employing a Zn-PCH (PVA chemical hydrogel) anode. J Solid State Electrochem

Zhang G, Liu X, Wang L et al (2019a) B, N-doped defective carbon entangled Fe3C nanoparticles as the superior oxygen reduction electrocatalyst for Zn–Air batteries. Acs Sustain Chem Eng 7:19104–19112

Zhang J, Zhang M, Zeng Y et al (2019b) Single Fe atom on hierarchically porous S, N-codoped nanocarbon derived from porphyra enable boosted oxygen catalysis for rechargeable Zn-Air batteries. Small 15:e1900307

Zhang Y, Guo Y, Liu T et al (2019c) The synergistic effect accelerates the oxygen reduction/evolution reaction in a Zn-air battery. Front Chem 7:524

Zhang J, Wang T, Xue D et al (2020) Energy-level engineered hollow N-doped NiS1.03 for Zn–Air batteries. Energy Storage Materials 25:202–209

Zhou T, Xu W, Zhang N et al (2019) Ultrathin cobalt oxide layers as electrocatalysts for high-performance flexible Zn-Air batteries. Adv Mater 31:e1807468

Zhu C, Ma Y, Zang W et al (2019) Conformal dispersed cobalt nanoparticles in hollow carbon nanotube arrays for flexible Zn-air and Al-air batteries. Chem Eng J 369:988–995